Magnetic susceptibility artifacts on high-resolution MR of the temporal bone.

M C Oehler, P Schmalbrock, D Chakeres and S Kurucay

AJNR Am J Neuroradiol 1995, 16 (5) 1135-1143
http://www.ajnr.org/content/16/5/1135

Magnetic Susceptibility Artifacts on High-Resolution MR of the Temporal Bone

Mary C. Oehler, Petra Schmalbrock, Donald Chakeres, and Saban Kurucay

PURPOSE: To determine whether signal variations and subtle anatomic deformities observed in high-resolution MR studies of temporal bones were caused by the large susceptibility differences at air-fluid interfaces near the round and oval window. **METHODS:** A systematic study of healthy subjects and plastic phantoms was conducted. The phantom consisted of a series of cylindrical holes of various small sizes within a solid block of plastic. These holes were partially filled with water and then covered with a reservoir of gelatin to simulate the otic capsule air-water interfaces. On a 1.5-T system, T2-weighted fast spin-echo images and three-dimensional Fourier transform gradient acquisition in steady state images were obtained using dedicated phased-array radio frequency coils. The directions of the frequency and in-plane phase-encoding gradients were swapped, and the receiver bandwidth was changed to demonstrate the dependence of the artifacts on these parameters. **RESULTS:** The phantom images confirmed and characterized artifacts consistent with magnetic susceptibility differences at the air-water interfaces. There is a combination of signal loss, misregistration in the frequency-encoding direction, and high signal foci related to the air-water interfaces. Furthermore, the artifacts were worse with narrower receiver bandwidth. Similar consistent artifact patterns were seen near the oval and round windows in studies of healthy subjects. **CONCLUSIONS:** In high-resolution MR imaging there are significant deformities in the display of the normal anatomy because of magnetic susceptibility.

Index terms: Magnetic resonance, artifacts; Temporal bone, magnetic resonance

AJNR Am J Neuroradiol 16:1135–1143, May 1995

Fast spin-echo (1) magnetic resonance (MR) and three-dimensional Fourier transform (2, 3) imaging techniques with phased-array surface coils (4) have allowed the development of high-resolution imaging of the temporal bone in routine clinical settings. Specifically, submillimeter resolution in all three spatial dimensions can be achieved with 3-D Fourier transform (3). These images of the temporal bone have dramatically improved the visibility of the small membranous labyrinth structures.

We have recognized consistently apparent anatomic deformities in these high-resolution images that are not associated with known anatomic structures of the membranous labyrinth (Fig 1). These distortions do not correlate with computed tomography (CT) imaging of the same structures and are seen as regions of adjacent high- and low-signal-intensity foci within the fluid-filled structures of the labyrinth (Fig 1). These findings are predominantly confined to regions adjacent to the oval and round windows. We hypothesize that the image deformities are related to magnetic susceptibility artifacts arising from fluid-air interfaces of the oval-round windows and the vestibule-cochlea.

The purpose of our study was to determine whether magnetic susceptibility could explain the changes seen on the images. To prove our hypothesis, we developed a phantom model that simulated the known anatomic fluid-air in-

Received August 31, 1994; accepted after revision January 24, 1995.
Funded in part by NIH Grant R29DC01646-01A1.
Dr Oehler received the American Society of Head and Neck Radiology's 1994 Head and Neck Radiologist in Training Award.
Presented at the International Congress of Head and Neck Radiology, Washington, DC, June 1994.

From the Departments of Radiology (M.C.O., P.S., D.C.) and Biomedical Engineering (S.K.), The Ohio State University, Columbus.
Address reprint requests to Mary C. Oehler, MD, Assistant Professor, Department of Radiology, Division of Neuroradiology, The Ohio State University, 410 W 10th Ave, Columbus, OH 43210.

AJNR 16:1135–1143, May 1995 0195-6108/95/1605–1135

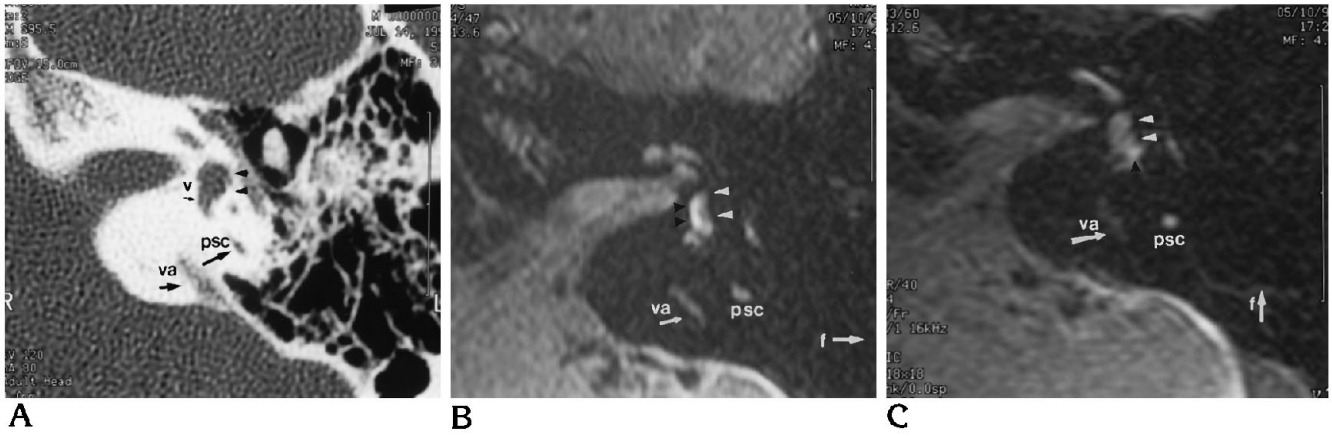

Fig 1. CT and MR comparison.

A, Axial high-resolution CT of the left temporal bone of a healthy volunteer at the level of the vestibule near the oval window niche. The normal vestibule (*v*) has a bulbous lateral margin toward the oval window (*small black arrowheads*). Normal labeled structures are the vestibule (*v*), vestibular aqueduct (*va*), and posterior semicircular canal (*psc*).

B, Axial MR gradient-echo sequence of vestibule in the same volunteer at very nearly the same level. The frequency-encoding direction is labeled with a *white arrow* (*f*). There is apparent flattening of the lateral margin near the oval window (*small white arrowheads*) and a bright linear focus of signal intensity (*curved white arrows*) within the vestibule that does not correspond to known structures within the otic capsule. We hypothesize that this is caused by magnetic susceptibility artifacts near the air-water interface of the oval window.

C, Axial MR gradient-echo image at the same level with the frequency-encoding direction oriented perpendicular to that of B (*f, white arrow*). Notice that the defect in the vestibule (*white arrowheads*) has a different configuration, as does the high-signal-intensity line (*singular curved white arrow*).

terfaces of the labyrinth and compared the phantom images with inner ear images of healthy subjects.

Methods

Initially, six volunteers (3 male, 3 female; range, 17 to 47 years of age) were studied with high-resolution 2-D fast spin-echo and 3-D gradient-echo imaging sequences. Subsequently, a phantom (Fig 2) and one volunteer were systematically evaluated to determine the origin of artifacts observed in the initial studies (Figs 3–7).

The phantom was made from a solid bar (13 × 2.5 × 2.5 cm) of clear plastic with cylindrical mechanically bored vertical 2-cm-deep holes varying in size from 1 to 5 mm drilled partially through the plastic bar (Fig 2). The vertical holes were partially filled with water on the bottom to indicate the location of the holes and to provide a cylindrical air-water interface. The upper portion of the vertically bored hole remained filled with air to the upper margin of the plastic bar. The air holes were covered with a thin plastic tape, and a tray was constructed and filled with gelatin solution, creating a second air-water interface at the lower margin of the gelatin reservoir (Fig 2). This phantom was designed to simulate the vestibule and its interfaces with air at the round and oval windows.

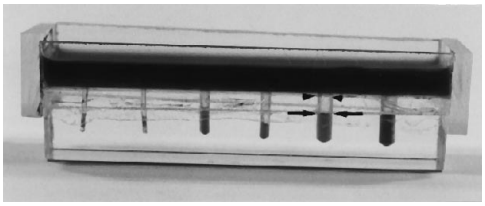

Fig 2. The plastic and water phantom. There are holes of varying size bored partly through the solid plastic bar. The holes are partially filled with water and the tray is filled with gelatin over the holes. The water has been colored for better visibility. This creates two air-water interfaces, one at the bottom of the tray (*arrowheads*) and the second at the top of the water column (*arrows*) in each bore.

High-resolution images were acquired with 2-D fast spin-echo and 3-D gradient-echo sequences using phased-array surface coils. We designed these coils for inner ear imaging (4) following previously described design criteria (5). Two semioval coils of 10 × 6.5 cm were overlapped such that the mutual inductance was minimal. Two such coils were constructed for bilateral use. High-resolution gradient-echo images were acquired using a 3-D Fourier transform gradient recalled acquisition in steady state (GRASS) with 24/61/1 (repetition time/echo time/excitations), 40° flip angle, 18 cm field of view, 512 × 288 matrix, and 60 sections of 1-mm thickness (voxel size, 0.35 × 0.63 × 1.0 mm). The acquisition time for these images was approximately 8 minutes. The images were obtained in the axial plane and could be reconstructed in any plane using the standard reconstruction software. T2-weighted fast spin-echo images were obtained with 6000/105/1, echo train length of 16, 18-cm field of view, 512 × 384 matrix, and no-gap interleaved 3-mm section thickness. The acquisition time was approximately 8 minutes.

For the phantom and two volunteers, separate images were obtained with the frequency-encoding gradients in the right/left and next anterior/posterior orientation, while keeping the other parameters constant (Figs 1, 3, 5, 6). Another set of images was obtained with different bandwidths of approximately 8, 16, and 32 kHz, keeping the other parameters constant (Figs 4, 5, 7).

The CT images were obtained on one volunteer using 1.5-mm section thickness at 1-mm intervals in the axial plane on a Hi-Lite Advantage General Electric CT scanner using a high-spatial-frequency (bone) algorithm (Fig 1). These images were obtained in image planes identical to the MR images for direct comparison. The CT images were obtained with a 512 × 512 matrix and 15-cm field of view using 80 mA and 140 kV. These images have a pixel size of 0.29 × 0.29 × 1.5 mm.

Results

Apparent artifacts occurred at water-air interfaces at the upper margin of the column of water in the bore of the phantom and at the air-gelatin interface at the undersurface of the gelatin reservoir. These artifacts varied with the direction of the frequency-encoding gradient (Fig 3).

With frequency encoding oriented parallel to the columns of water, at the upper margin of the water columns, there was exaggeration of the apparent meniscus, with a high signal region in the center of the column (Fig 3). At the base of this meniscus, there was a higher-signal-intensity focus within the water column. The deformity of the undersurface of the gelatin-air interface was a symmetrically shaped signal defect in the expected flat water surface. The shape of the defect was approximately semicircular, but there was a bulge of signal into the crescent centrally (Fig 3A). A bright line of signal intensity was present along the outer margin of the signal void within the high signal intensity of the gelatin.

When the frequency-encoding direction was perpendicular to the water columns, the artifacts changed their configuration (Fig 3B). The upper margins of the water columns were not symmetric and appeared to be asymmetrically displaced along the frequency-encoding direction. The shape of the meniscus signal void became asymmetric when the frequency-encoding direction was oriented left-right. The high-signal-intensity focus was shifted horizontally (Fig 3B), and in fact the lateral margin of the hole within the plastic was distorted and appeared stretched to the left side. The undersurface of the gelatin reservoir also was deformed. The regions of signal void were smaller and more asymmetric than when the frequency-encoded gradient was parallel to the bored holes. A bright focus of signal intensity was seen adjacent to the known location of the air-water interface to the left.

With the wider bandwidth (32 kHz), the artifacts were less pronounced than with the narrower bandwidths (8 and 16 kHz), but the gen-

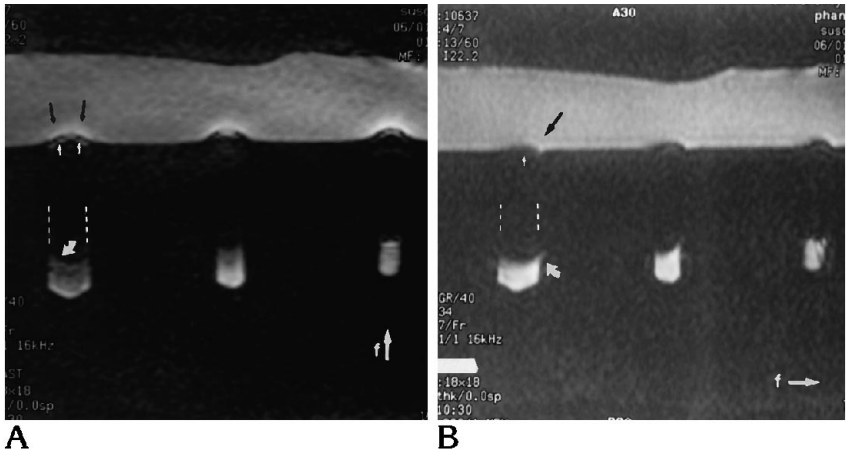

Fig 3. Swapping the frequency-encoding directions.

A, Gradient-echo images of the phantom (Fig 2) obtained in a plane parallel to the bored holes (coronal). The frequency-encoding direction is oriented parallel to the column of water (*f, vertical white arrow*). The *dotted white lines* demonstrate the location of the air-filled bore that is a signal void. There is a large semicircular signal void (*small white arrows*) at the undersurface interface of the gelatin and the air within the column. Adjacent to the signal void is a high-signal-intensity line (*small black arrows*). Also note the meniscus is exaggerated at the upper margin of the water in the bore (*curved white arrow*).

B, This image is obtained in an identical fashion except that the frequency-encoding gradient is oriented perpendicular to the column of water (*f, white horizontal arrow*). There is an asymmetric void within the gelatin reservoir at the air-water interface (*small white arrows*). A high-signal-intensity focus is seen shifted to the left margin of the air-gelatin interface near the signal void (*black arrow*). The upper surface of the water column in the bored hole is also asymmetrically distorted, with apparent displacement to the left (*curved white arrow*).

eral characteristic shapes of the artifacts were unchanged (Fig 4).

These findings were true for both the fast spin-echo and the 3-D Fourier transform images, but the areas of signal void were more pronounced on the gradient-echo sequences, as would be expected with magnetic susceptibility (Fig 5). The high-signal-intensity regions were more pronounced on the fast spin-echo than the gradient-echo images. The distortion of the sides of the bored holes was more apparent on the fast spin-echo images of the phantom (Fig 5). The quality of the 8-kHz-bandwidth gradient-echo images was very poor, so comparison was limited.

The artifacts were visible on both fast spin-echo and gradient-echo images, but in general were more severe on the gradient-echo images than on the fast spin-echo images (Fig 5). One exception to this was on the fast spin-echo phantom images with the frequency-encoding gradient oriented perpendicular to the column of water. On these fast spin-echo images, the distortion of the walls of the bored tubes in the plexiglas was much more apparent than on the gradient-echo images. This may be related to section thickness and a section-selection gradient susceptibility effect. On the fast spin-echo images, the high-signal-intensity foci were the predominant finding, whereas on the gradient-echo images, the signal voids were larger and more pronounced than the higher-signal-intensity foci.

On the volunteer subjects, the artifacts and distortion near the site of the oval window was most easily evaluated and will be primarily discussed. The basal turn of the cochlea adjacent to the round window also was affected and did not have its normal bulbous appearance. The changes at the round window will not be discussed in detail.

Consistent regions of high and low signal variation were seen within the vestibule near the oval window. These artifacts were always in a characteristic direction. Adjacent to the high-signal-intensity foci was an area of signal loss causing distortion and truncation of the expected bulging margin of the vestibule near the oval window (Fig 1). These characteristic signal voids along the margin of the vestibule were very reproducible and were observed for both fast spin-echo and gradient-echo techniques. The exact pattern of deformity changed in coincidence with the changes in frequency-encoding direction (Fig 6). The artifacts were anteroposterior in their orientation with respect to the images when the frequency encoding direction was right-left. A high-signal-intensity stripe was seen within the vestibule, with an adjacent low-signal-intensity band near the truncated vestibule facing the oval window. The pattern in the right ear was very similar to the pattern in the left ear.

The artifacts were right-left oriented lines on the image when the frequency-encoding direction was anteroposterior in orientation with respect to the images and were symmetric for both ears. The deformity near the oval window with truncation of the normal shape was not as apparent with frequency oriented anteroposterior (Fig 6).

Volunteer images obtained with multiple bandwidths of approximately 8, 16, and 32 kHz in a manner identical to that of the phantom images showed similar changes in the artifacts. The artifacts were more pronounced for the narrower (8 and 16 kHz) bandwidths than for the wider bandwidth of 32 kHz (Fig 7). However, on

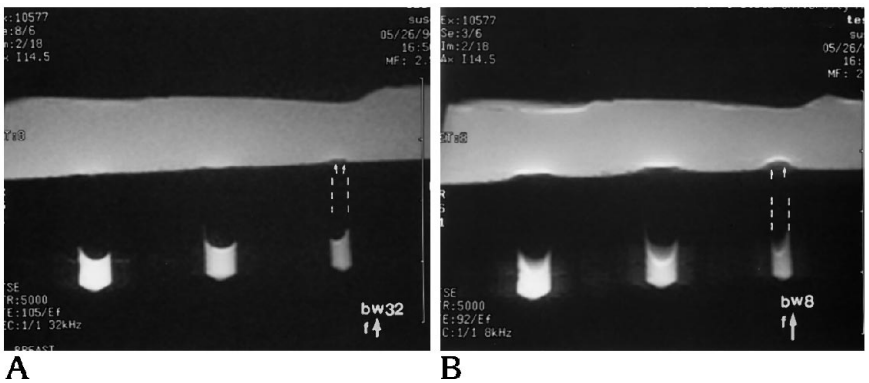

Fig 4. Comparison of the multiple bandwidths.

A, Fast spin-echo phantom image with 32-kHz bandwidth. The *dotted lines* parallel the margin of the air-filled bore. It demonstrates a small area of signal void at the undersurface of the gelatin reservoir and air interface (*small white arrows*).

B, Image obtained in an identical fashion except with an 8-kHz bandwidth. It demonstrates a larger area of signal void at the undersurface of the water reservoir and air interface (*small white arrows*). The apparent lengthening of B compared with A is caused by misregistration (ie, the signal is misplaced along the frequency-encoding direction).

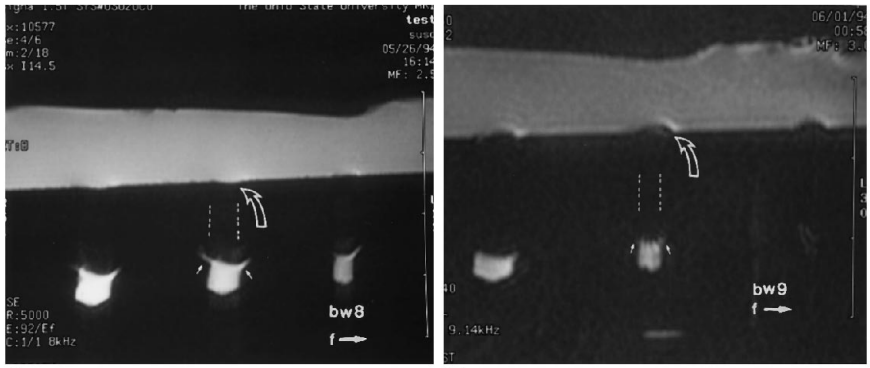

A B

Fig 5. Comparison of gradient-echo and fast spin-echo phantom images.

A, Fast spin-echo phantom image with bandwidth of 8 kHz. The frequency-encoding gradient (*f, white arrow*) is oriented perpendicular to the bored holes. This image demonstrates distortion of the lateral margins of the water within the bore (*small white arrow*) as well as minimal distortion of the inferior surface of the gelatin (*curved white arrow*).

B, Gradient-echo image of the same phantom with 9-kHz bandwidth. Frequency is oriented perpendicular to the bored holes. This demonstrates less distortion of the lateral margins of the hole than is seen with the fast spin-echo images (*small white arrows*), but greater distortion of the inferior surface of the gelatin (*curved white arrow*). The height of the large tube appears reduced on B because of dephasing effects near the air-fluid interface. The width of the middle tube is reduced on the gradient-echo images because the sections are thinner than in the fast spin echo, and the tube is cylindrical with more volume averaging on the fast spin-echo images. The small tube is not included in the depicted section of the gradient-echo image but can be seen on the adjacent image.

the fast spin-echo images, the anatomic detail of the cerebrospinal fluid spaces was better, with the narrower bandwidths. The direction of the artifact depended only on the frequency-encoding direction, but the magnitude of the abnormality was larger with the narrower bandwidth. For example, with a 32-kHz bandwidth and right-left oriented frequency, the vestibule was nearly normal in shape with only a small focus of increased signal intensity in the vestibule (Fig 7A). With a bandwidth of 8 kHz, the signal void along the margin of the vestibule and the focus of higher signal intensity within the vestibule were much larger. On the fast spin-echo 8-kHz bandwidth images, as compared with the 32-kHz bandwidth, the detailed anatomy of the nerve fibers within the internal auditory canal was improved, but there was loss of brain–cerebrospinal fluid contrast (Fig 7A).

Discussion

Magnetic field strength variations (ie, field inhomogeneities) and gradient-field nonlinearities are major sources of image artifacts and distortions. Magnetic field inhomogeneity is not only dependent on the quality of the instrument magnet, but also on the magnetic susceptibility of the material inserted in the magnetic field.

Magnetic susceptibility artifacts are most prominent at interfaces between tissues with different susceptibilities. These differences in magnetic susceptibility cause small but significant local field variations. For in vivo imaging, interfaces between water containing tissue-air and soft tissue–bone have most pronounced susceptibility differences. However, air has a much greater impact on the local field than bone (6). Therefore, the most pronounced artifacts are seen at air-fluid interfaces. The exact

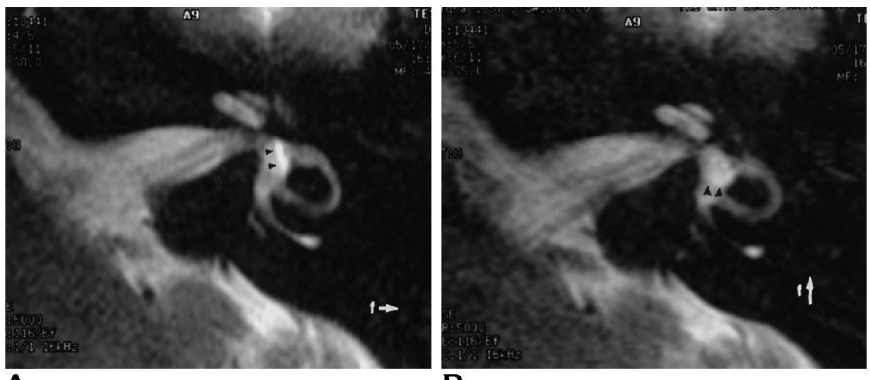

A B

Fig 6. Swapping frequency-encoding gradients in the volunteer study.

A, Fast spin-echo image of a volunteer's left temporal bone with the frequency-encoding gradient oriented right-left (*f, white arrow*). This demonstrates a focus of high signal intensity in the lateral vestibule (*black arrowheads*) above the oval window.

B, Fast spin-echo image, identical except that the frequency-encoding gradient is oriented anteroposterior (*f, white arrow*). This demonstrates a high-signal-intensity line that is oriented horizontally (*black arrowheads*) in the posterior vestibule.

shape and orientation of the interface plays an important role as well. For example, for a cylindrical rod-shaped air column (of infinite length), surrounded by water, oriented perpendicular to the external magnetic field, the susceptibility field can be exactly computed. With this information, it is possible to explain why a circular object appears as an arrowhead (6). The magnetic susceptibility field distortion in our phantom study is more complex. Prediction of the local field deformities is more complicated and the resulting image deformities are less symmetric. Even more complex susceptibility field deformities are present at the air-fluid interfaces near the round and oval windows in the inner ear. As an example, this can be directly observed with image acquisition methods that are very sensitive to magnetic field inhomogeneities (2).

In summary, the exact shape of the structures, differences in their susceptibilities, and orientation in the external magnetic field all influence the local susceptibility field and thus the final image appearance. It is important to note that local susceptibility field variations do not change with time, provided the structures with different susceptibility fields do not move.

Image Effects from the Susceptibility Field

The interaction of the local susceptibility field changes near the interfaces, and the spatial-encoding gradients influence the final image appearance. The effects are different for the frequency, phase, and section-selection gradients.

Effects in Frequency-Encode Direction. The artifacts caused by magnetic susceptibility are in part analogous to chemical-shift artifacts in that they both represent interfaces leading to differences in the precessional frequency of the spins (6). These frequency variations then are translated into variations on the image causing misplacement of signal (Figs 3, 6). As seen in the familiar chemical-shift artifacts at fat-water interfaces, this results in an area with relatively increased signal intensity and one with relatively decreased signal intensity (7). Thus both chemical shift and susceptibility lead to signal misplacement and geometric distortions in gradient-echo and spin-echo images. The magnitude of the frequency differences caused by magnetic susceptibility are in the range of chemical-shift differences. As for chemical shift, the magnetic susceptibility effects are more pronounced with higher-field-strength magnets because of larger Larmor frequency differences.

With magnetic susceptibility artifacts, an analogous misregistration occurs at the interfaces between tissues of different magnetic susceptibility. However, unlike chemical shift, which results in only a few specific frequencies (eg, two frequencies for fat and water), susceptibility fields lead to a wide range of different frequencies with a complex spatial distribution. Unlike for chemical-shift artifacts, the signal shifts can be in opposite directions within a very narrow space. For example, if the signal is shifted toward a region that has signal, such as the vestibule, then an unusual higher-signal-intensity focus within the vestibule will be seen (Fig 6). If the signal is shifted toward a region of signal void, the signal decreases. At the bone-air interfaces, the shifts are not seen because no signal is seen for air or bone.

In our phantom and volunteer images, when the frequency-encoding direction is changed, the magnetic susceptibility artifacts shift their

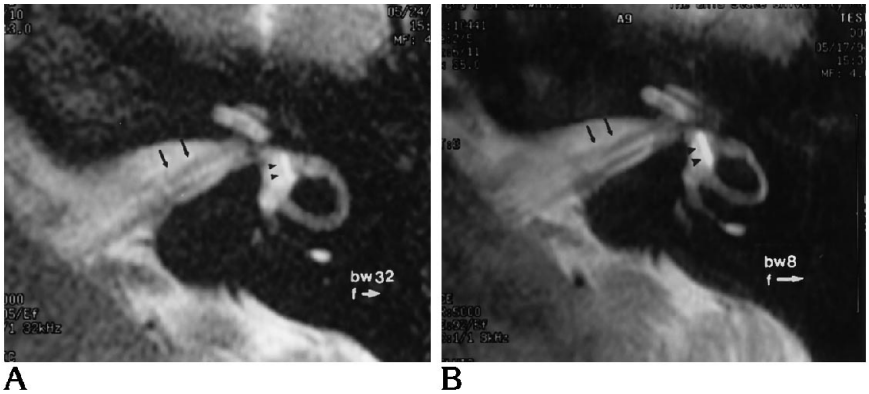

Fig 7. Varying the bandwidth with volunteer study.

A, Left temporal bone fast spin-echo section of a healthy volunteer, acquired with a 32-kHz bandwidth. *B* was acquired with an 8-kHz bandwidth and a horizontal frequency-encoding gradient (*f, white arrow*). These images demonstrate that with an increasing bandwidth (32 kHz) there are smaller apparent artifacts (*small black arrowheads*). Decreasing bandwidth (8 kHz) yields larger artifacts. However, with increased bandwidth, there is less detail of the nerve structures within the internal auditory canal because of lower signal-to-noise ratio (*black arrows*).

orientation in a manner similar to chemical shift. If the frequency-encoding direction is right-left with respect to the images, the artifacts are predominately anteroposterior in orientation (Fig 6A). When the frequency-encoding direction is changed to be anteroposterior in orientation, the artifacts are more right-left oriented (Fig 6B). We did demonstrate findings similar to earlier reports in that the artifacts shifted with the changing of the frequency-encoding direction. This can be a useful tool to reduce deformities in pituitary imaging, for example, where air–soft tissue interfaces occur at the floor of the sella (8).

Bandwidth. The receiver bandwidth is an important parameter associated with frequency encoding that affects the image appearance. The bandwidth is the range of frequencies that is selected for digitization of the signal. Increased bandwidth is linked with shorter sampling times and faster signal reception times. This decreases the signal-to-noise ratio because fewer data are collected. Wider bandwidths frequently are used for fast imaging sequences at the expense of signal-to-noise ratio (9). Narrow bandwidths have slower sampling times and thus longer readout time. This increases signal-to-noise ratio. Narrow bandwidth imaging also requires longer echo time, because of the longer gradients required for the longer readout time. Both our phantom and our volunteer images demonstrated this dependence of image detail on receiver bandwidth.

In addition, the bandwidth affects the appearance of susceptibility artifacts. For example, if an image signal is digitized with the bandwidth of $\pm$32 kHz and 512 point, this corresponds to 125 Hz per pixel. For digitization with $\pm$8 kHz and 512, the frequency resolution is 31 Hz per pixel. For a susceptibility field that causes, for example, a 60-Hz shift in precessional frequency, the signal is shifted by about two pixels for the narrow bandwidth, but only one half pixel for the wide bandwidth. Therefore, susceptibility misregistration is much more pronounced for low-bandwidth than for high-bandwidth images. Again, this is analogous to chemical-shift effects.

This numerical example also can illustrate why susceptibility misregistration artifacts play a more important role for high-resolution imaging. Susceptibility field and, thus, frequency differences are large only in the close vicinity of the interface. For larger distances, the susceptibility field difference decreases rapidly. Because magnetic susceptibility is an inherent tissue parameter, it is impossible to suppress completely. If the shape of the structure is known before it is imaged, the changes in the field can be partially suppressed by calculation and filtering techniques (10); however, current correction methods may not be suitable for routine clinical imaging. It also is impossible to shim for such small, complex, nonlinear field deformities, which are much smaller than bulk magnetic susceptibility effects.

Effects in Phase-Encoding Direction. Susceptibility effects do not cause geometric distortions in the phase-encode direction. Again, this is analogous to chemical shift. The reason for this is that susceptibility fields (and chemical shift) do not change with time. Thus, while the local field differences cause variations in precessional frequencies, this difference is identical for each phase-encoding step. Consequently, there is no net effect and no shift in the phase-encode direction. Because susceptibility fields lead to signal misplacement in the frequency-, but not the phase-encoding, direction, interchanging of the phase and frequency directions leads to the observed differences in image appearance.

Effects in the Section-Selection Direction. Susceptibility field variations near interfaces can superimpose with the section-selection gradient fields and this can lead to misplacement of the excited region on the final image. Depending on the orientation of the section-selection gradient and the susceptibility field distortion, some areas within the section may not be excited, leading to signal void in the section. Alternatively, spins outside the section may be excited, leading to extra signal in some locations. This effect is important, predominantly for thin-section 2-D imaging. For example, in the 2-D fast spin-echo phantom images presented in this study, the susceptibility fields at the air-water interface of the bored holes may create frequency shifts such that spins outside the image section are excited. This may explain the increased prominence of spatial distortion at the air-fluid interface of the bored holes on the fast spin-echo versus the gradient-echo images (Fig 5). For 3-D imaging this effect is less important, because a thick slab containing the entire temporal bone is excited. Thus, the local frequency shifts caused by susceptibility should all fall within the frequency range of the excitation

pulse. As discussed above, the section phase encoding does not lead to shifts.

Dephasing Effects. In addition to the geometric distortions described thus far, susceptibility effects are especially prominent with gradient-echo images because of additional effects of intravoxel phase dispersion (6). Because of the strong local variation of the susceptibility field, spins with a wide range of precessional frequencies are present within one voxel. This leads to dephasing and thus, to signal loss. Again this dephasing is somewhat analogous to the fat/water out of phase effect in gradient-echo images. The major difference is that only two different chemical-shift frequencies are present for water and fat, leading to dephasing only for specific echo times. In contrast, susceptibility causes a range of frequencies and thus signal loss for all sufficiently long echo times. Therefore, as an alternate but equivalent way, susceptibility dephasing can be described by a T2* relaxation time. T2* is shorter than the tissue intrinsic T2, thus yielding lower signal for a given echo time. Susceptibility dephasing artifacts can theoretically be reduced by decreasing echo time. Decreasing echo time is limited, however, by the strength and speed of the system's gradients. We are currently pursuing new strategies to decrease echo time on the gradient-echo sequence to reduce the dephasing effects (11).

Reduction of Susceptibility Artifacts

Magnetic field inhomogeneities and gradient-field nonlinearities are a major source for image artifacts and distortions. The gradient field nonlinearity can be corrected by improved gradient coil design or by mathematical correction of the image data with the known gradient linearity profile, and the homogeneity of the static field can be improved by shimming. However, because magnetic susceptibility is an inherent tissue parameter, complete suppression of artifacts is not easy, if not impossible, in a clinical setting. Shimming for such localized, complex, nonlinear field deformities is not an option with standard low-order shim gradient coils. Mathematical corrections algorithms were proposed (10, 12), but require a priori knowledge of the shape of the structures. Such knowledge generally is not available in a clinical setting. We are currently working on an alternate approach to reduce susceptibility misregistration artifacts by using systems theory (Kurucay S, presented at the 2nd meeting of the Society of Magnetic Resonance, 1994).

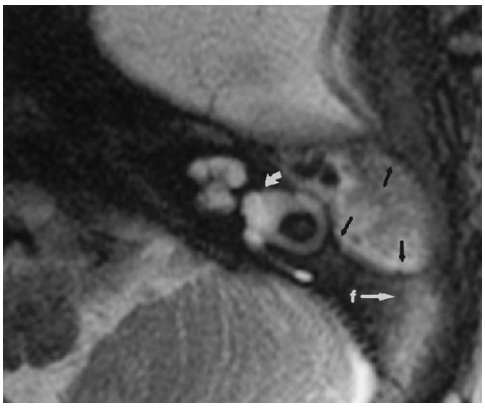

Fig 8. Lack of artifacts with opacification of the middle ear cavity. This axial fast spin-echo image is of a patient with congenital deformity of the inner ear. There is opacification of the middle ear cavity by mucous (*small black arrows*). Notice that the high-signal-intensity deformity of the vestibule is not demonstrated (*curved white arrow*) near the oval windows. We speculate that the fluid within the middle ear obliterates the air-water interfaces near the oval window. Therefore, the artifacts of the interfaces are not seen.

Conclusion

In summary, our study shows that susceptibility artifacts exhibit noticeable effects in high-resolution imaging of the membranous labyrinth both for 2-D fast spin-echo and 3-D GRASS imaging. Additional signal loss caused by dephasing is observed in the gradient-echo images. It is important to recognize such artifacts and not mistake them for disease.

As with some other artifacts observed in MR, the presence or absence of artifacts actually may be used to provide diagnostic information. Although the described susceptibility artifacts were observed in all studies of healthy subjects, artifacts were not observed in one case, in which fluid filled the middle ear. If there is fluid or tissue filling the middle ear adjacent to the windows, these artifacts are not seen (Fig 8). This observation leads to interesting implications for future imaging. Perhaps with fenestral otosclerosis, we will be able to make the diagnosis based on the lack of artifacts near the oval window when bone replaces air. Furthermore, the identification of cerebrospinal fluid fistulas may be made, not because of high signal within the fistula, but because of magnetic susceptibility artifacts from air in an unusual location.

References

1. Tien RD, Felsberg GJ, Ferris NJ, et al. Fast spin-echo high resolution MR imaging of the inner ear. *AJR Am J Roentgenol* 1992; 159:395–398
2. Schmalbrock P, Brogan MA, Chakeres DW, et al. Optimization of submillimeter-resolution MR imaging methods for the inner ear. *J Magn Reson Imaging* 1993;3:451
3. Tien RD, Buxton RB, Schwaighofer BW, Chu PK. Quantitation of structural distortion of the cervical neural foramina in gradient echo MR imaging. *J Magn Reson Imaging* 1991;1:683
4. Schmalbrock P, Pruski J, Sun L, Rao A, Monroe JW. Phased array RF coils for high resolution MRI of the inner ear and brain stem. *J Comput Assist Tomogr* 1995;19:8–14
5. Hayes CE, Tsuruda JS, Mathis CM. Temporal lobes: surface coil phased-array MR imaging. *Radiology* 1993;189:918–920
6. Bakker CJG, Bhagwandien R, Moerland MA, Fuderer M. Susceptibility artifacts in 2DFT spin-echo and gradient-echo imaging: the cylinder model revisited. *Magn Reson Imaging* 1993;11:539–548
7. Soila KP, Viamonte M Jr, Starewicz PM. Chemical shift misregistration effect in magnetic resonance imaging. *Radiology* 1984; 153:819–820
8. Sakurai K, Fujita N, Harada K, Kim SJW, et al. Magnetic susceptibility artifact in spin-echo MR imaging of the pituitary gland. *AJNR Am J Neuroradiol* 1992;13:1301–1308
9. Crooks LE, Hoenninger J, Arakawa M, Watts J, et al. High-resolution magnetic resonance imaging. *Radiology* 1984;150:163–171
10. Sumanaweera TS, Glover GH, Binford TO, Adler JR. MR susceptibility misregistration correction. *IEEE Transactions on Medical Imaging*, June 1993;12:No. 2
11. Ying K, Schmalbrock P, Clymer B. Echo-time reduction for submillimeter resolution imaging with a 3D phase encode time reduced acquisition method. *Magn Reson Med* 1995;33:82–87
12. Sumanaweera T, Glover G, Song S, Adler J, Napel S. Quantifying MRI geometric distortion in tissue. *Magn Reson Med* 1994;31: 40–47